The Fermi Gases and Superfluids: Short Review of Experiment and Theory for Condensed Matter Physicists

K. Levin

James Franck Institute
The University of Chicago
Chicago, 60637, Ill.

Randall G. Hulet

Department of Physics and Astronomy
Rice University
Houston, Texas 77005

Abstract

The study of ultracold atomic Fermi gases is a rapidly exploding subject which is defining new directions in condensed matter and atomic physics. Quite generally what makes these gases so important is their remarkable tunability and controllability. Using a Feshbach resonance one can tune the attractive two-body interactions from weak to strong and thereby make a smooth crossover from a BCS superfluid of Cooper pairs to a Bose-Einstein condensed superfluid. Furthermore, one can tune the population of the two spin states, allowing observation of exotic spin-polarized superfluids, such as the Fulde Ferrell Larkin Ovchinnikov (FFLO) phase. A wide array of powerful characterization tools, which often have direct condensed matter analogues, are available to the experimenter. In this Chapter, we present a general review of the status of these Fermi gases with the aim of communicating the excitement and great potential of the field.

Keywords: dilute quantum gas, Fermi gases, BCS-BEC Crossover, superfluidity

Email addresses: `levin@@control.uchicago.edu` (K. Levin), `randy@@rice.edu` (Randall G. Hulet)

Contents

1. Introduction

The Fermi gases and the Fermi superfluids represent a new class of condensed matter "materials." Aside from their neutrality and the fact that they appear in confined geometries (traps), they possess many essential features found in strongly correlated systems. Adding to the excitement is the fact that these systems are highly tunable. We will see below that one can dial-in

the strengths of interactions (both repulsive and attractive), the size and geometry of the (optical) lattice, spin polarizations, as well as other features. The milestones in this discovery phase were the creation of a degenerate Fermi gas (1999), the formation of dimers of fermions (2003), Bose-Einstein condensation (BEC) of these dimers (late 2003) and finally, condensation of fermionic pairs (2004). Many challenges were met and surmounted in the process and within a remarkably short period of time, researchers were able to observe a new form of "high temperature" superconductivity (in the sense of large T_c/E_F) and to develop a set of tools to characterize this new state of matter. The available set of tools is equally remarkable. The experimental complexity of these ultracold Fermi gases can not be over-stated. It is not possible to use traditional thermometers to measure temperature, nor attach leads on a sample (in a current-voltage set up) to measure the superconducting gap. Nevertheless, the experimental community has devised ways of doing these analogue condensed matter experiments, as well as the analogue of photoemission, transport, neutron scattering and "magnetic field" experiments. We touch on all of these briefly in this Chapter.

The extensions of these experiments to optical lattices will be discussed in Chapter 5. But even in studies of trapped gases without lattices, which are the focus here, there are exciting opportunities for insights into many physics sub-disciplines. This is based on interest in (i) the strong interaction limit, known as the unitary gas (see Chapter 6) and (ii) the related smooth evolution of superfluidity from fermionic (BCS) to bosonic (BEC). Interest in the first of these has captured the attention of scientists who also work on quark-gluon plasmas, as well as in nuclear and astrophysics. The BCS-BEC crossover has captured the attention of condensed matter physicists who contemplate implications for high temperature superconductivity.

1.1. Theory Summary and Overview

The background theory for this Chapter focuses on fermionic superfluidity and the unusual "normal" states which are present above the transition temperature. The physics is relatively simple to appreciate. Fermionic superfluidity is driven by an attractive interaction between fermions which leads them to pair up and thereby introduces boson-like degrees of freedom. These bosons, called "Cooper pairs", are driven by statistics to condense at low temperatures, and in the process form a superfluid state. In the simplest case, the "Bose condensation" is a macroscopic occupation of a many particle ground state in which the net pair momentum is zero. A formal machinery

3

BCS

BEC

weak coupling

strong coupling

large pair size
k-space pairing

small pair size
r-space pairing

strongly overlapping
Cooper pairs

ideal gas of
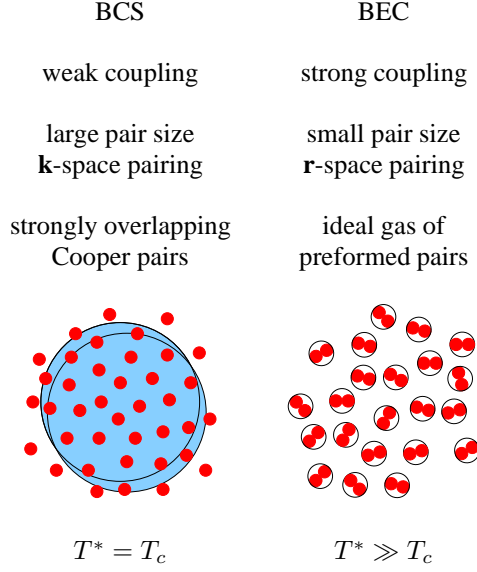preformed pairs

$T^* = T_c$

$T^* \gg T_c$

Figure 1: Contrast between BCS- and BEC-based superfluids

for implementing this picture was presented by Bardeen, Cooper and Schrieffer (BCS) and it has worked remarkably well for addressing conventional superconductors as well as superfluid helium-3. With the discovery of the high temperature superconductors there was a re-examination of BCS theory, not so much because it failed in the well studied superconductors, but because it began to emerge as a very special case of a much more general theory.

This more general theory of fermionic superfluids is known as BCS-Bose Einstein condensation (BEC) or BCS-BEC theory. This approach identifies BCS theory with the limit of extremely weak attractive interactions. This weak attraction is associated with very loosely bound pairs. We refer to the pair size as the "coherence length" ξ so that these BCS pairs are in the limit of very large coherence length compared to the interparticle spacing. This identification corresponds well with the behavior of ξ which is directly observed in conventional superconductors. As the attraction becomes stronger, the pairs become more tightly bound. Since the superfluid onset temperature, T_c, is directly related to this attraction, it is simultaneously increased.

While there is a smooth crossover between BCS and BEC superfluids, the physics changes most dramatically when one studies the behavior above T_c. Here, once one leaves the BCS (weak attraction) regime, the normal phase
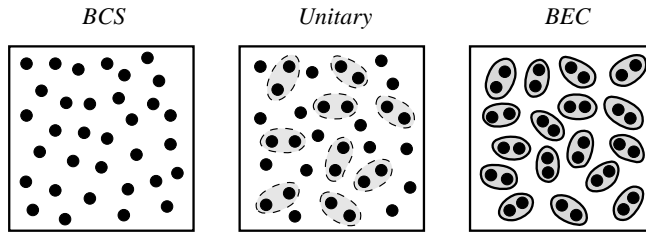
Figure 2: Schematic illustration of excitations (both above and below the transition T_c) in the BCS, unitary and BEC regimes. The single black discs represent fermionic excitations. Pair excitations (represented by two fermions) become progressively dominant as the system evolves from the BCS to BEC regime.

changes from fermionic to a more bosonic character. How does one monitor this change in effective statistics? This is possible through a parameter known as the pairing gap, Δ. The pairing gap is the energy one must provide to break up the Cooper pairs and create separate fermions. We emphasize the pairing gap parameter in our theoretical discussions.

The cold Fermi gases have provided a unique opportunity to study the BCS-BEC crossover because one can continuously tune the attractive interaction via Feshbach resonances. The literature has focused on the so-called unitary regime which is roughly mid-way between BCS and BEC. This regime corresponds to a particular interaction strength in which the two body scattering is associated with a divergent scattering length $a \to \infty$. One could view this limit as the most strongly interacting regime [1]. Deep in the BCS side the interactions (between fermions) are weak and deep on the BEC side the interaction (between tightly bound bosons) are similarly weak. Indeed, many different physics sub-disciplines have been interested in the unitary gas, which is more extensively discussed in Chapter 6. One might also imagine that high temperature cuprate superconductors belong to this more general category of BCS-BEC. Supporting this scenario is the fact that ξ is anomalously small, and T_c is, of course, high. In addition, there is a rather extensive body of evidence that the normal state has a non-zero pairing gap. This is frequently referred to as the "pseudogap."

We begin with an introduction to the qualitative picture of the BCS-BEC crossover scenario which is represented schematically in Figure 1. This figure shows the contrasting behavior of the two endpoints. An important parameter in the literature is T^* which is the crossover temperature where pairs first start to form. In the usual BCS theory, the attractive interactions
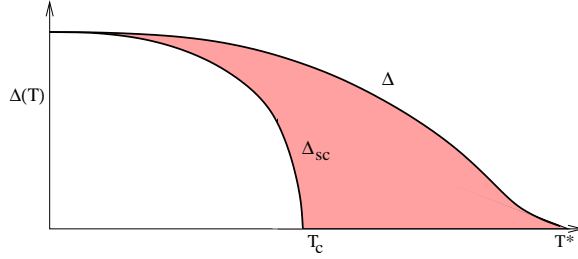
5

Figure 3: Contrasting behavior of the excitation gap $\Delta(T)$ and superfluid order parameter $\Delta_{sc}(T)$ versus temperature, appropriate to the unitary regime. The height of the shaded region roughly reflects the density of noncondensed pairs at each temperature.

are so weak that there is no pairing until condensation occurs, so that $T^* \approx T_c$, while in the BEC limit $T^* >> T_c$.

In Fig. 2 we present a schematic plot of the nature of the excitations (fermionic, bosonic, or some mix of the two), as one varies from BCS to BEC. These are present both above and below T_c, the latter as excitations of the condensate. Midway between BCS and BEC (i.e., in the unitary regime) there will be a mix of fermions and quasi-long lived bosons. These bosons and fermions are not separate fluids, but rather they are strongly inter-connected. Indeed, the gap in the fermionic spectrum (related to Δ) is a measure of the number of bosons in the system.

In Fig. 3 we show a schematic of the gap parameter $\Delta(T)$ as a function of T, along with the superfluid order parameter $\Delta_{sc}(T)$. The former, which represents the "bosonic" degrees of freedom, shows that pairs continuously form once the temperature is less than a crossover temperature T^*, while the order parameter turns on precisely at T_c. The height of the shaded region in this figure reflects the number of noncondensed pairs. This number increases monotonically with decreasing T, until T_c is reached. As T further decreases below T_c the number of noncondensed pairs begins to decrease monotonically due to the condensation of zero momentum pairs.

1.2. Creating Quantum Degenerate Fermi Gases

The achievement of Bose-Einstein condensation of trapped atomic gases in 1995 was a watershed event in the history of many-body physics [2, 3, 4, 5]. Since then, an astounding number of phenomena, described in Chapter 2 of this volume, have been explored with atomic bosons. Within just a few months of these first experiments, a proposal to use ^{6}Li to experimentally
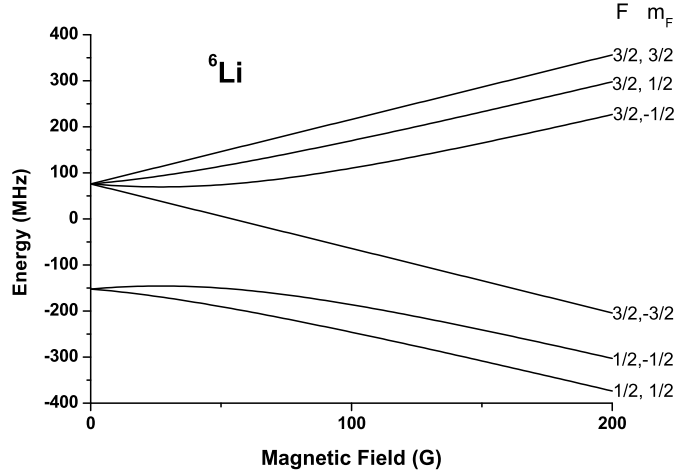
Figure 4: Hyperfine sublevels of the ^{6}Li $2S_{1/2}$ ground state. The labels on the the right indicate the total electronic angular momentum F and its projection m_F, which are both good quantum numbers at low fields. At higher fields, the three most energetic levels correspond to electron spin-up, while the three lowest to electron spin-down. The two lowest-going sublevels, with $m_F = \pm 1/2$, exhibit a broad Feshbach resonance near 834 G.

realize Cooper pairing in an atomic Fermi gas was published [6]. While s-wave interactions are forbidden between fermionic atoms in the same internal state due to the Pauli exclusion principle, interactions are allowed in a two-component Fermi gas. This pseudo-spin-1/2 system of atomic fermions can be realized using two of the ground-state hyperfine sublevels, which are shown in Fig. 4 for ^{6}Li. These sublevels differ in either electronic or nuclear spin projection. The early proposal showed that the naturally large attractive interaction between the two uppermost (most energetic) sublevels in ^{6}Li was sufficient for pairing to occur at temperatures that had already been achieved in the boson experiments. However, two-body inelastic collisions are unacceptably large for these sublevels. A better choice is the two *lowest* sublevels of ^{6}Li, which are energetically stable. Furthermore, a Feshbach resonance could be used to tune their relative interaction strength to essentially *any* value [7]. Indeed, the collisional stability of a two-component Fermi system near a Feshbach resonance substantially exceeds that of a Bose gas. Feshbach resonances have turned out to be essential for experiments on Fermi superfluidity, both in ^{40}K and ^{6}Li; they will be discussed in more detail in the next section.

Creating degenerate Fermi gases proved to be not quite as straightfor-

ward as it was for the Bose gases, described in Chapter 1. The final cooling step in every successful quantum gas experiment with ultracold atoms has been evaporative cooling. Here, the most energetic atoms are removed from the gas leaving the remaining atoms to rethermalize to a lower temperature. This process can be very efficient, but it requires these thermalizing collisions to repopulate the high-energy tail of the Boltzmann distribution. As we've seen above, however, a Fermi gas must contain at least two spin-states (hyperfine sublevels) in order for such collisions to occur, and the additional state opens up more pathways for inelastic loss. Since all early quantum gas experiments utilized magnetic trapping, a further constraint was that the two sublevels had to be "weak-field seeking", such that the energy of the state increases with field. Accommodating evaporative cooling without unacceptably high atom loss from these inelastic pathways proved to be considerably more difficult for fermions than for bosons.

Several methods were developed to circumvent the evaporative cooling problem. The first degenerate Fermi gas was produced at JILA in 1999 using ^{40}K [8], which has an unusually large nuclear spin of 4. Because of the large nuclear spin in ^{40}K, there are several weak-field seeking sublevels in the lower, more stable manifold, and a gas formed from two of these was magnetically trapped and evaporated to degeneracy. This approach was not available for ^{6}Li since its nuclear spin is only 1. Another approach was developed for ^{6}Li in which a single spin-state is cooled "sympathetically" using a co-trapped but entirely different atomic species. This was employed at Rice and at ENS in Paris using ^{7}Li as the refrigerant atom [9, 10]. The actively evaporated ^{7}Li cools the ^{6}Li by collisions, which are not symmetry forbidden. Figure 5 shows how the *in situ* column densities of the two species evolve as evaporation progresses. Even though the two isotopes are co-trapped in the same volume their optical transition wavelengths are sufficiently different that the two species can be independently imaged. Initially, both species are relatively hot and their distributions are essentially the same. Importantly, as the atoms get colder, it is clear that the fermions occupy a larger volume than do the bosons. This is an effect of Fermi pressure, the same mechanism that stabilizes white dwarf stars against gravitational collapse.

1.3. Feshbach Resonances

The Feshbach resonance has played a central role in achieving pairing in ultracold atomic Fermi gases. No experiment has thus far demonstrated pairing without employing a Feshbach resonance to create a sufficiently strong at-
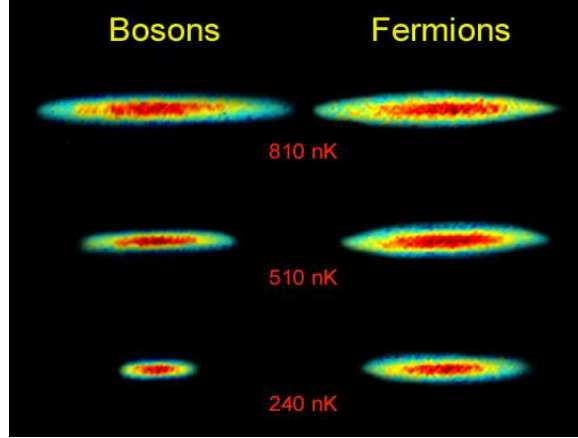
Figure 5: Sympathetic cooling of fermionic ^{6}Li by bosonic ^{7}Li. The ^{7}Li atoms are actively evaporated using an RF method, while the ^{6}Li is sympathetically cooled via elastic collisions. The three different temperatures shown, corresponding to the three rows, are obtained by modifying the evaporation cycles appropriately. A separate laser beam is used to image each isotope. (Data from Ref. [9])

tractive interaction. Furthermore, the realization of the BEC-BCS crossover relies on tuning the interaction strength between atoms from strongly binding in the BEC regime to weakly attractive on the BCS side. The simplest way to conceptualize such tunability is to imagine that the interaction between two non-identical fermions is a square well with tunable depth U. The interaction can be described by the s-wave scattering length a. For very small U, such that the well is unable to support bound states, a is small and negative, corresponding to a small attractive interaction. This is the BCS regime where the transition temperature $T_c \sim \exp(-1/k_F a)$ is exponentially small. Here, k_F is the Fermi wavevector, and $k_F a$ is the natural unit of interaction strength. As U is increased, a remains negative but increases in magnitude until at sufficiently large U the square well finally supports a bound state. This point corresponds to a scattering resonance where a goes from $-\infty$ to $+\infty$, and is termed the "unitarity" limit, where the scattering cross section is maximum. For even larger U, a remains positive but diminishes in magnitude.

While this simple "single-channel" model gives the flavor of the Feshbach resonance, it is incomplete. The Feshbach resonance actually involves two-channels, usually corresponding to the singlet ($S = 0$) and triplet ($S = 1$) interaction potentials between pairs of ground-state alkali-metal atoms [11].
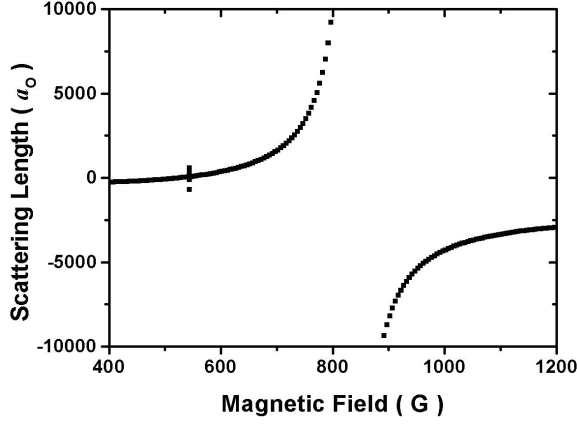
9

Figure 6: Coupled channels calculations of the ^{6}Li Feshbach resonances involving the energetically two lowest Zeeman sublevels. A broad resonance is located near 834 G, while a narrow one can be discerned near 543 G [12].

The total electronic spin, S, is only an approximately good quantum number, as the singlet and triplet states are coupled by the hyperfine interaction. A Feshbach resonance occurs when atoms in the "open" ($S = 1$) or scattering channel, are near resonance with a bound state in the "closed" ($S = 0$) channel. If the open and closed channels have different magnetic moments, the resonance can be tuned magnetically. A good example is ^{6}Li, whose two lowest sublevels (Fig. 4) go through resonance near 800 G [7], as shown in Fig. 6. At a field of 834 G the scattering continuum of the open channel is resonant with the bound singlet. At higher fields there is no bound state possible, only an attraction that gives rise to pairing in the BCS regime. But at fields below resonance the superposition of the triplet continuum with the singlet bound state gives rise to a weakly-bound molecular state, whose binding energy scales as $1/a^2$. Sufficiently far below resonance, the molecular size ($\sim a$) will be small compared with the average interparticle distance, giving $k_F a \ll 1$. This is the BEC regime where the molecules condense into a Bose superfluid at low temperature.

2. Establishing Pair Condensation and Superfluidity in Cold Fermi Gases

One should appreciate that temperature is not straightforward to measure in these cold gases. Moreover, because they are neutral and have a normal
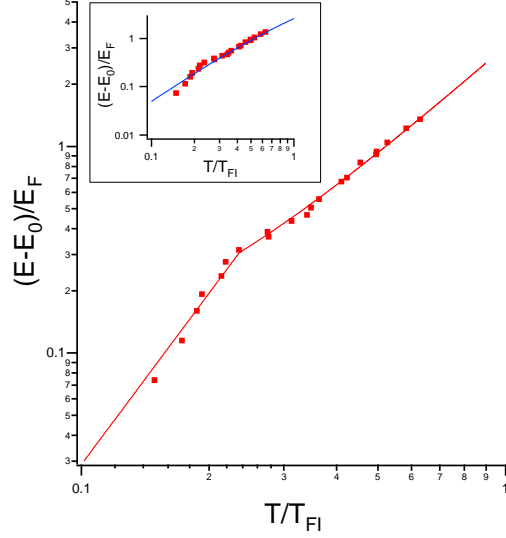
10

Figure 7: Evidence for a phase transition (presumably to the superfluid phase) via plots of the energy E for a trapped gas vs. physical temperature T. The blue line in the inset corresponds to the BCS or essentially free Fermi gas case, and the red data points to unitarity. The slope change of the latter indicates a phase transition. T_{FI} is the Fermi energy of an ideal Fermi gas, and because these are measurements with a trapped gas, $T_c \approx 0.23$ differs from the theoretical value obtained for a homogeneous gas of $T_c \approx 0.15 - 0.17$. Adapted from Ref. [17].

state gap, it is difficult to convincingly establish that one has a superfluid phase. Initial strong indications of pair condensation were first obtained on the BEC side of resonance [13, 14], where there are clear bimodal signatures in the density profile. This bimodality (i.e., separation between condensate and excited atoms) is the hallmark of Bose superfluids. The density profiles at unitarity, however, have essentially none of this bimodality. The earliest indications of condensation at unitarity came a few months later [15, 16] via fast magnetic field sweep experiments which start at unitarity and project onto the BEC regime (where condensation is more evident in the particle density profiles). The presumption is that even if the condensate fraction is not conserved upon a fast sweep to BEC, the presence or absence of a condensate will be preserved [15, 16]. The time frame for the sweep will not allow a condensate to form in the BEC regime if there were none present near unitarity, nor will it allow a condensate to disappear if it was present initially.
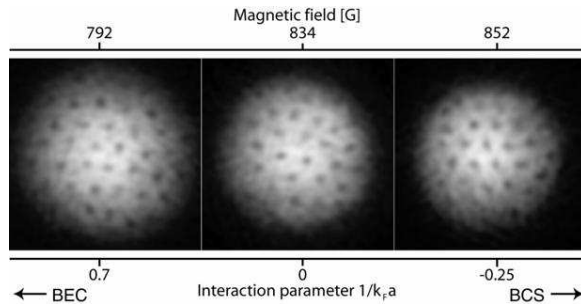
11

Figure 8: Evidence [18] for fermionic superfluidity via quantized vortices, from BCS to BEC.

The second generation experiments were based on thermodynamical measurements. Figure 7 shows evidence for a phase transition as reported in Ref. [17]. The measured energy is plotted as a function of temperature. The key feature here is that the data (indicated by the solid circles) show an abrupt change at a temperature one can call T_c. This abrupt change occurs for the unitary scattering case. No such feature is seen for the noninteracting Fermi gas.

The last generation experiment to make the case for superfluidity was the rather stunning observation of quantized vortices by the MIT group [18], which is shown in Fig. 8. Although, these also involve sweeps to the BEC regime, to obtain sufficient contrast in the images, they provide the most direct evidence for superfluidity in the unitary gases.

3. Theory Outline

In contrast to the Bose gases, there is no consensus theory as yet to describe these Fermi superfluids. Considerable effort has gone into both many body analytic schemes as well as Monte Carlo and related numerical approaches. Measures of what constitutes a "successful" theory differ from one sub-community to another. From a condensed matter perspective one tends to look for novel physical effects and focus on conceptual issues relating, for example to other highly correlated systems. Nevertheless, the universality which appears precisely at unitarity, and the history of precision measurements associated with the atomic physics community tend to favor theoretical schemes which make quantitative contact with experiment.

In this Chapter we restrict our consideration to analytical studies which build on the simplest (BCS) theory of conventional superconductors. This

is largely because BCS theory represents, perhaps, the most complete and accessible analytical theory we have in condensed matter physics. We will see below that the form of the ground state wavefunction associated with the BCS-BEC crossover is the same as that introduced in the original BCS theory. One has the hope, then, of being able to construct a theory of the crossover in as complete a fashion as the 1957 theory of Bardeen, Cooper and Schrieffer. This is not to say that the ultimate theory of the unitary gas is expected to be fully captured by this mean field approach, but it nevertheless should provide some useful intuition.

The field of BCS-BEC crossover is built around early observations by Eagles [19] and Leggett [20] that the BCS ground state is much more general than was originally believed. If one increases the strength of the attraction and self-consistently solves for the fermionic chemical potential μ (which eventually decreases from the Fermi energy to negative values), the wave function corresponds to a more BEC-like form of superfluidity. This ground state is given by the standard BCS wavefunction,

$$\Psi_0 = \Pi_{\mathbf{k}}(u_{\mathbf{k}} + v_{\mathbf{k}} c^\dagger_{\mathbf{k},\uparrow} c^\dagger_{-\mathbf{k},\downarrow})|0\rangle \,, \tag{1}$$

where $c^\dagger_{\mathbf{k},\sigma}$ and $c_{\mathbf{k},\sigma}$ are the creation and annihilation operators for fermions of momentum $\mathbf{k}$ and spin $\sigma = \uparrow, \downarrow$. The variational parameters $v_{\mathbf{k}}$ and $u_{\mathbf{k}}$ are associated with the number of occupied and unoccupied pair states, respectively.

3.1. *Theory of Finite Temperature Effects: Comparing BCS and Ideal Boson BEC*

It is useful to base our intuition of fermionic superfluids on that of true Bose gas condensation. The bosonic degrees of freedom appearing in the BCS wavefunction Eq. (1) are associated with fermionic pairs. Pair-pair interactions are not explicitly present so one could say these Cooper pair bosons are essentially ideal. Since an ideal Bose gas cannot support superfluidity, the superfluidity in the BCS case (as established, say, by the Meissner effect) implies that fermionic substructure of the bosons is necessary and sufficient to sustain superfluidity. For ideal point bosons one uses the condition that the total number of bosons is the sum of the condensed contribution $N_0(T)$ and the excited contribution $N'(T)$ with $N = N_0(T) + N'(T)$. Moreover, the latter is straightforward to calculate

$$N'(T) = \sum_{\mathbf{q} \neq 0} b(\Omega_q) \tag{2}$$

13

where $b(\Omega_q)$ is the usual Bose-Einstein function written in terms of the non-condensed bosonic excitation spectrum $\Omega_q \propto q^2$. Converting this to a density of states integral one has, following Chapter 2,

$$N'(T) = \int_0^\infty d\epsilon \, \frac{g(\epsilon)}{\exp[\beta(\epsilon - \mu_B)] - 1} \tag{3}$$

which defines the total number of particles not in the condensate. Here $g(\epsilon)$ is the density of states per unit volume for bosons with $\epsilon \propto q^2$ dispersion and ϵ_0 is the single particle ground state energy which we take to be zero, as in Chapter 2. The equality $\mu_B(T, N) = 0$ is a fundamental constraint for all $T \leq T_c$. The condensate fraction N_0 is obtained from $N - N'(T)$.

To arrive at the fermionic counterpart of the above equations, we need to formulate a generalized many body theory. A number of such schemes have been introduced in the literature but we begin with one which is consistent with Eq. (1) and with finite temperature extensions associated with Gor'kov and Bogoliubov-de Gennes theory. The simplest extension of BCS theory to address the crossover can be summarized via the following equations. As with the ideal Bose gas one implements a constraint, on the non-condensed fermion pairs which, below T_c are in chemical equilibrium with the condensate

$$\mu_{pair} = 0, \qquad T \leq T_c \,. \tag{4}$$

Importantly, if the non-condensed pairs are properly identified, this leads to the familiar BCS equation for the pairing gap

$$\Delta(T) = -U \sum_{\mathbf{k}} \Delta(T) \frac{1 - 2f(E_{\mathbf{k}})}{2E_{\mathbf{k}}} \,, \tag{5}$$

where $E_{\mathbf{k}} = \sqrt{(\epsilon_{\mathbf{k}} - \mu)^2 + \Delta^2(T)}$, and $f(E_{\mathbf{k}})$ is the usual Fermi function. We may decompose the excitation gap into two contributions

$$\Delta^2(T) = \Delta_{sc}^2(T) + \Delta_{pg}^2(T), \tag{6}$$

where $\Delta_{sc}(T)$ corresponds to condensed and $\Delta_{pg}(T)$ to the non-condensed gap component. Just as in the Bose case, the number of non-condensed bosons is determined from the dispersion of the non-condensed pairs which must be compatible with Eq. (5) and yields

$$\Delta_{pg}^2(T) = Z^{-1} \sum b(\Omega_q, T) \,. \tag{7}$$

14

Here Z is a coefficient of proportionality (unimportant for our purposes) which can also be determined microscopically. It should be stressed that while $\Delta^2(T)$ plays a similar role in the fermionic system to the total bosonic particle number N, the former is generally temperature dependent (except in the extreme BEC limit.) Finally, not only does one need the bosonic chemical potential (for bosons in equilibrium with the condensate), but the fermionic chemical potential of the excited fermions must be established in the usual way via the well known number equation.

$$ n = \sum_{\mathbf{k}} \left[1 - \frac{\epsilon_{\mathbf{k}} - \mu}{E_{\mathbf{k}}} + 2\frac{\epsilon_{\mathbf{k}} - \mu}{E_{\mathbf{k}}} f(E_{\mathbf{k}}) \right] , \qquad (8) $$

In this way, as follows from Eq. (6), the onset of superfluid coherence or non-zero Δ_{sc} is associated with the condition that the gap equation cannot be satisfied by having only non-condensed pairs. We emphasize that $\Delta^2(T)$ plays an analogous role to the number of bosons N, and this should underline the fact noted earlier that $\Delta \neq 0$ is really the only way to get a handle on the bosonic degrees of freedom in a fermionic system.

3.2. Analytic Formalisms for Addressing Fermi Gas Experiments

What is particularly distinctive about the Fermi gases as compared to their Bose counterparts is the fact that the former can be studied throughout the entire range of temperatures and, moreover, one finds the expected second order phase transition at T_c. For the Bose gases, theories are mostly confined to very low T and, when extended, lead to a first order phase transition at T_c. In Chapter 2 we saw that a well developed tool for addressing experiments in the cold Bose gases was the Gross-Pitaevskii (GP) theory which could be used in both time independent and time dependent situations. In order to apply the theoretical ideas discussed above to experimental situations in the Fermi gases, where there are spatial dependencies, one has three main analytical tools. (i) Landau-Ginsburg theory which is the fermionic analogue of Gross-Pitaevskii theory which describes the condensate and (ii) Gor'kov theory and (iii) Bogoliubov-de Gennes theory. The last two describe the fermionic excitations of the condensate but become more complicated when one includes non-condensed bosons. An additional analytical tool which is of widespread utility is linear response theory to address weak perturbations of the superfluid. An analytical many body approach to BCS-BEC schemes lends itself to implementation of linear response theory, provided one does

this in a consistent, conservation-law-respecting way. The larger number of theoretical options for the Fermi gases as compared with their Bose counterparts reflects the fact that they contain three rather than two components: fermionic excitations, pair excitations and condensate contributions. In strict BCS theory the situation is simpler since there are no pair excitations, while in strict BEC theory there are no fermionic excitations.

We saw in Chapter 2 that the (Bose gas) *condensate* dynamics is given by

$$i\hbar\frac{\partial\Psi_B(\boldsymbol{r},t)}{\partial t} = \left[-\frac{\hbar^2\nabla^2}{2M} + V_{\text{tr}}(\boldsymbol{r}) + g|\Psi_B(\boldsymbol{r},t)|^2\right]\Psi_B(\boldsymbol{r},t), \qquad (9)$$

where Ψ_B now depends on t as well as on $\boldsymbol{r}$. A similar equation can be written for Fermi gas, although here one should be careful to address both the dynamics of the condensate as well as that of the non-condensed pairs. For both of these, one writes rather generally the same equation as for the bosons, but with a different pre-factor on the left

$$(e^{i\theta}) \times \hbar\frac{\partial\Psi_F(\boldsymbol{r},t)}{\partial t} = \left[-\frac{\hbar^2\nabla^2}{2M} + V_{\text{tr}}(\boldsymbol{r}) + g|\Psi_F(\boldsymbol{r},t)|^2\right]\Psi_F(\boldsymbol{r},t), \qquad (10)$$

This equation is known as the time-dependent Landau-Ginsburg theory, which has been derived microscopically for the condensate only near T_c and in the BCS regime. Here one finds a diffusive dynamics in contrast to the behavior of the time dependent bosonic Gross Pitaevskii behavior, albeit primarily associated with very low temperatures. Thus, the factor $e^{i\theta}$ is purely real for the fermionic condensate in this temperature regime. Here the bosons are not well established or long-lived. Deep in the BEC regime of fermionic superfluids the dynamics associated with the non-condensed pairs is such that $e^{i\theta}$ is purely imaginary, corresponding to stable, long lived bosons which have a propagating dynamics. More generally, between BCS and BEC this factor is a complex number and θ may be viewed as varying with the strength of the attractive interaction.

By far the most straightforward way of including trap inhomogeneity effects is the local density approximation (LDA). This approximation assigns the properties of a non-uniform fermionic system at a given point their bulk values with an effective local chemical potential. Then the calculations proceed as in a homogeneous system with the replacement

$$\mu(\boldsymbol{r}) = \mu_o - V_{\text{tr}}(\boldsymbol{r}), \qquad (11)$$

16

	Cold Fermi gases	Condensed Matter
Gap Measurements	Radio Frequency Spectroscopy	Tunneling Measurements
Fermionic Dispersion	Momentum Resolved Radio Frequency	Angle Resolved Photoemission
Scattering Measurements	Bragg two-photon scattering	Neutron Scattering
Transport Measurements	Viscosity and Spin Transport	Conductivity dc and ac
Magnetic Field Studies	Critical Rotation Frequency	Upper Critical Magnetic Field

Table 1: Summary of the analogous experimental probes used in trapped atomic gases and their counterparts in condensed matter.

where $V_{\mathrm{tr}}(\boldsymbol{r})$ represents the confining potential. Here the fermionic chemical potential $\mu(\boldsymbol{r})$ can be viewed as varying locally but self consistently throughout the trap and μ_o is the chemical potential at the trap center. For the most part, this approach has been useful for addressing thermodynamic properties in a trap.

4. Experimental Tools

A remarkable series of advances have made it possible to find experimental counterparts to many of the most powerful tools we have in condensed matter physics. These are outlined in Table 1 below. In the next few subsections we discuss how these are implemented and some of the observations based on these techniques.

4.1. Measuring the Pairing Gap

Experiment and theory have worked hand in hand in developing an understanding of the so-called radio frequency (RF) "pairing gap spectroscopy" in the atomic Fermi gases. This class of experiments was originally suggested as a method for establishing the presence of superfluidity [21, 22]. Pairing gap spectroscopy is based on using a third atomic level, called $|3\rangle$, which does not participate in the superfluid pairing. Under application of RF fields, one component of the Cooper pairs, called $|2\rangle$, is excited to state $|3\rangle$. If there

is no gap Δ then the energy it takes to excite $|2\rangle$ to $|3\rangle$ is the atomic level splitting ω_{23}. In the presence of pairing (either above or below T_c) an extra energy Δ must be input to excite the state $|2\rangle$, as a result of the breaking of the pairs.
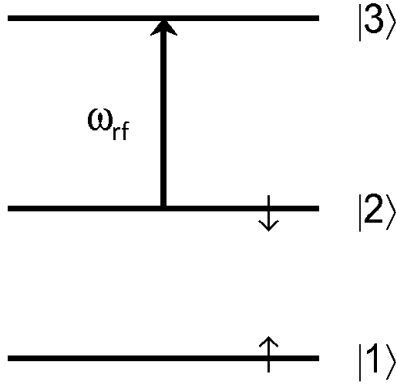

Figure 9: Experimental configuration for radio frequency spectroscopy.

A ground breaking experimental paper [23] reported the first experimental implementation of this pairing gap spectroscopy in ^{6}Li over a range of fields corresponding to the BCS, BEC and unitary regimes. Accompanying this paper was a theoretical study [24] based on the BCS-BEC crossover approach introduced earlier [25], but, importantly, generalized to include trap effects. Indeed, because of trap effects measurements of the pairing gap are not entirely straightforward to interpret. At general temperatures, a measurement of the current out of state $|2\rangle$ is associated with two discrete structures. A sharp peak at $\omega_{23} \equiv 0$ which derives from "free" fermions at the trap edge and a broader peak which reflects the presence of paired atoms; more precisely, this broad peak corresponds to the distribution of Δ in the trap. At high T (compared to Δ), only the sharp feature is present, whereas at low T only the broad feature remains. Additional experiments have introduced a powerful way of exploiting and enhancing RF spectroscopy using tomographic techniques [26]. Here the RF contribution is resolved at different distances from the trap center, throughout the trap. This spatial distribution is obtained using in-situ phase-contrast imaging and 3D image reconstruction. In this way, scans at different trap radii yield an effectively

homogeneous spectrum.

These data alone do not directly indicate the presence of superfluidity, but rather they provide evidence for pairing. Indeed, like photoemission in condensed matter systems, these measurements reflect the fermionic spectral function $A(\mathbf{k}, \omega)$. One caveat should be noted here. Unlike a photoemission experiment where the fermion is removed from the sample, here it is excited to a higher internal energy state. As a consequence there may be residual interactions between atoms in this excited state and the non-excited ("Cooper pair partner") states in the system. These are known as final state effects, which can, fortunately, often be minimized.

4.2. Momentum Resolved Radio Frequency Experiments: A Cold Gas Analogue of Angle Resolved Photoemission

Recent experiments on ^{40}K from the JILA group [27] have demonstrated that it is possible to measure spectral functions directly using momentum resolved RF pairing gap spectroscopy over a range of magnetic fields throughout the BCS-BEC crossover. These experiments are able to resolve the kinetic energy E_k, and thereby, the three-dimensional momentum distribution of the RF-excited (or "out-coupled") state 3 atoms. Since the momentum of the RF photon is effectively negligible, the momenta of the out-coupled atoms can be used to deduce that of the original 1-2 paired state. There is a substantial advantage of using ^{40}K for these studies over the more widely studied ^{6}Li since there are no nearby Feshbach resonances involving the final state for ^{40}K that complicate interpretation of the spectra. Momentum resolved RF spectra can be compared with momentum resolved (or "angle resolved") photoemission in the high temperature superconductors. The goal of these experiments and related theory is to deduce the fermionic quasi-particle dispersion, which would reveal the pairing gap $\Delta(T)$.

In Fig. 10 we present experimental measurements of the one particle fermionic spectral functions as a contour plot. The dotted white curve represents an estimate of the experimentally deduced peak dispersion, which can then be fit to the BCS dispersion involving $E_{\mathbf{k}}$, which was introduced below Eq. (5). With higher resolution it should be possible to obtain more direct information about the mean experimentally-deduced gap size. Importantly, the fact that the experiments were done near T_c has been argued to suggest that there is a sizable pseudogap in the Fermi gases at and above T_c in the unitary regime.
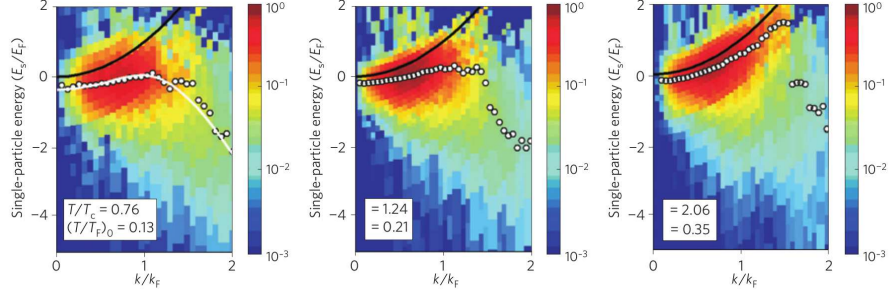
19

Figure 10: Momentum resolved radio frequency ("Photoemission") spectra [28] throughout the pseudogap regime. These spectra are for Fermi gases at three different temperatures, each with roughly the same interaction strength, near unitarity.

4.3. Universal Properties: The Closed Channel Fraction and the Contact

Strongly interacting Fermi gases exhibit a universality, as discussed in Chapter 6, that extends their significance beyond that of any particular realization, such as cold atoms, atomic nuclei, or even quark matter. At unitarity, the absence of any length scale other than the particle density implies that there is a direct proportionality between the chemical potential and the Fermi energy of a non-interacting gas. The coefficient of proportionality, known as the Bertsch parameter, governs the low energy properties of the system. Short distance correlations, characterized by a parameter $\mathcal{C}$, known as the "contact", have also been shown to be related to a broad array of universal properties [29, 30, 31]. $\mathcal{C}$ connects quantities as diverse as the high-momentum tail of the momentum distribution (including the high frequency tail of RF spectra), the total energy, the rate of change of total energy with respect to an adiabatic change in a, and a virial theorem relation [29, 30, 31]. These universal relations are particularly powerful as they extend beyond unitarity into the BCS and BEC regimes, connect microscopic quantities to thermodynamic ones, and require only that $|a|$ be large compared to the scale of the interaction potential.

$\mathcal{C}$ can be directly measured by determining the strength of the local pair correlations, which was done using photoassociation [32]. We saw in section 1.3 that Cooper pairs in these systems are a superposition of the triplet scattering state (open channel) and a bound vibrational level of the singlet potential (closed channel). For ^{6}Li, the bound $S = 0$ vibrational level corre-

sponds to $v = 38$, and the pairs can be expressed as

$$|\psi_{\mathrm{p}}\rangle = Z^{1/2}|\psi_{v=38}(S = 0)\rangle + (1 - Z)^{1/2}|\phi_{\mathrm{a}}(S = 1)\rangle, \qquad (12)$$

where Z is the closed-channel fraction. Here, $\psi_{v=38}(S = 0)$ are the closed-channel molecules and $\phi_{\mathrm{a}}(S = 1)$ are the free atom pairs in the triplet channel. In the case of wide resonances, and the ^{6}Li resonance is as wide as any known Feshbach resonance, Z is expected to be small throughout the resonance region. For sufficiently small Z, the resonance may be well described by a universal single-channel model, such as the square-well discussed previously. Under these conditions, the macroscopic properties of the superfluid are independent of the microscopic physics of the two-body interactions.

The quantity Z has been measured experimentally for ^{6}Li using photoassociation [32]. Since S is a good quantum number in the vibrational levels of the Li$_2$ molecule, the selection rule $\Delta S = 0$ is obeyed in the photoassociation transition. The singlet part of the pairs can then be picked out by driving an optical transition from $|\psi_{\mathrm{p}}\rangle$ to an electronically-excited molecular state with $S = 0$. The rate of such an excitation will be proportional to Z, where the proportionality depends on the constant bound-bound matrix element between $|\psi_{v=38}(S = 0)\rangle$ and the excited molecule. An excitation results in a detectable loss of trapped atoms. The rate of excitation was measured in this way and the corresponding values of Z were determined throughout the BEC-BCS crossover, as shown in Fig. 11. At unitarity, $Z < 10^{-4}$, and Z remains smaller than 1%, even deep into the BEC regime. These results confirm the universality for broad resonances.

It was pointed out in Ref. [32] that since the rate of photo-excitation in this experiment is proportional to the overlap between two tightly bound molecular levels of the Li$_2$ molecule whose sizes are much smaller than typical interparticle distances, it is also proportional to the integral over volume of the local pair correlation $G_2(r, r) = \langle \hat{\psi}_{\downarrow}^{\dagger}(r)\hat{\psi}_{\uparrow}^{\dagger}(r)\hat{\psi}_{\uparrow}(r)\hat{\psi}_{\downarrow}(r)\rangle$, where $\hat{\psi}_{\uparrow}$ and $\hat{\psi}_{\downarrow}$ are the fermionic field operators for atoms in different internal states. Consequently, a measurement of Z also corresponds to a measurement of the short-range pair correlations. Furthermore, since the integral over volume of $G_2(r, r)$ is proportional to the contact $\mathcal{C}$ introduced by Tan in Refs. [29, 30], the measurement of the closed-channel fraction is a measurement of the contact [33, 34].

Several of the other contact relations have been recently experimentally verified [35]. In these measurements, $\mathcal{C}$ was obtained from measurements as
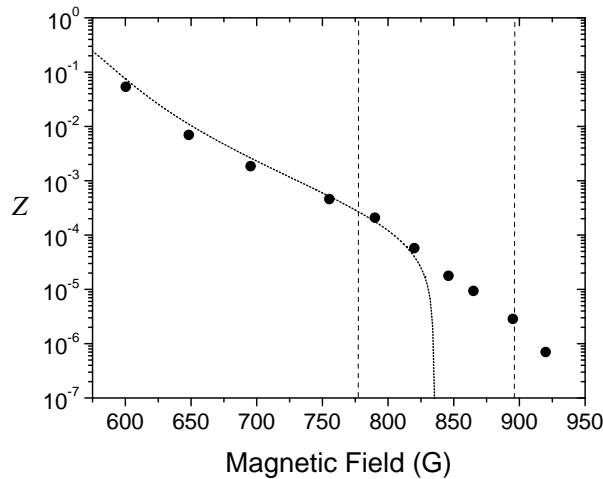
Figure 11: Closed-channel fraction Z throughout the BEC-BCS crossover. The closed circles represent the value of Z extracted from the rates of photo-excitation to an excited molecular level. The dotted line shows a comparison with results obtained from an exact (coupled channels) two-body calculation. The vertical dashed lines represent the boundaries of the strongly-interacting regime, $k_F|a| > 1$. (Reprinted from Ref. [32])

.

diverse as the high-momentum tail of the momentum distribution obtained by releasing the atoms from a trap, to thermodynamic quantities such as a generalized virial relation.

4.4. Thermodynamics

The thermodynamic variables, energy, pressure, and entropy, have been systematically studied for the unitary gases. The earliest such measurements established trap averaged quantities [17], such as plotted in Fig. 7. These measurements have been reanalyzed using a new determination of temperature, independent of theory. More recently [36], there has been considerable progress in establishing the equation of state or the thermodynamic potential, $\Omega = -PV$, for a homogeneous gas. This is based on the local density approximation and a simple relation between the local pressure inside a trapped gas and the twice integrated density profiles, or "axial density". Here temperature is usually determined by using the surface density as a thermometer. A single image gives the pressure as a function of variable chemical potential, thereby providing a large number of independent determinations of the equation of state. By collecting and averaging the data from many such images, one obtains the equation of state with very low noise. Figure 12 shows a
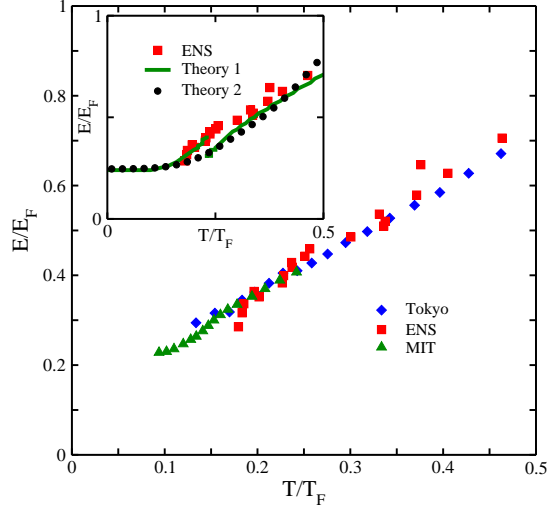
22

Figure 12: Comparison of different equations of state for the energy E versus temperature measured experimentally and labeled ENS [36], Tokyo [37] and MIT [38]. The inset presents predictions from two theory groups denoted 1 [39] and 2 [17], respectively, as compared with one set of experimental data [36]. The equations of state in some instances have been updated with new thermometry. The Theory "2" plots include a fitted Hartree term and Theory "1" is based on a modified Nozieres Schmitt-Rink approach [40].

comparison of recent data from three different groups as well as examples of theoretical plots in the inset. This figure should make it clear that thermodynamic studies (there are counterparts for entropy, chemical potential, etc.) have received considerable attention in the cold atom community.

Of considerable interest in these thermodynamic experiments are universal properties associated with unitarity. In this infinite scattering length case (with an interaction of zero range) the energy per unit volume of the system is directly proportional to that of the free Fermi gas at the same density n.

$$\epsilon(n) \equiv \frac{E}{V} \propto \frac{n^{5/3}}{m} \equiv \xi \epsilon_{free}(n) \tag{13}$$

Here ξ is the "Bertsch" parameter which is independent of any materials parameters, applying equally to all Fermi systems at unitarity. This parameter appears to be around 0.38 within about 2 %.

Experiments are close to converging on these thermodynamical characterizations of both the trapped and homogeneous gases. The equations of state

for the latter, in particular, have been viewed as important benchmarks for assessing numerical and analytical approaches to the Fermi gases. Nevertheless it should be stressed that thermodynamical probes are not as discriminating tests of theory as are dynamical probes. This is most readily seen by comparing transport properties (say, the shear viscosities) of fermionic vs bosonic quantum fluids, helium-3 and helium-4 [41], with their specific heat counterparts. Here one sees that the latter are far more similar than are the viscosities. Using thermodynamics as a precision test of theory may be incomplete and it is extremely important to provide a characterization of transport in the ultracold Fermi gases, as well. This lays the groundwork for the focus on the dynamics in unitary gases which is discussed in Chapter 6.

4.5. Transport Experiments in the Fermi Gases

We summarize briefly these viscosity measurements to be discussed in Chapter 6. These experiments deduce the shear viscosity from the damping of collective (breathing) modes in the trapped gas. A great deal of interest has focused on viscosity experiments because they seem to reflect "perfect fluidity", as is expected in many strongly interacting systems, such as quark-gluon plasmas. One can ask about the counterpart of perfect fluidity in condensed matter superconducting systems. Indeed the conductivity at any low frequency ω except strictly zero is a close analogue to viscosity. This conductivity is associated with the excited states of the condensate and must be distinguished from the infinite conductivity of the condensate itself which occurs at $\omega = 0$. Despite the fact that the condensate contribution to conductivity is infinite, (while the condensate contribution to viscosity is zero), the analogies hold between the contributions to transport from the condensate *excitations*. A perfect fluid has anomalously low viscosity, while a bad metal has anomalously low conductivity. This "bad metallicity" is widely studied in the high temperature superconductors [42].

Recent viscosity data are plotted in Chapter 6 for a unitary trapped Fermi gas [43]. The viscosity and its ratio to entropy density are both observed to be strongly suppressed at low T as was theoretically predicted [44]. The normal state behavior is in contrast to what is expected of a Fermi liquid. The superfluid behavior is more similar to (fermionic) helium-3 but in contrast to what would be expected in superfluid (bosonic) helium-4. The behavior of both helium-3 and the Fermi gases can be understood as reflecting the strong reduction in the number of *fermionic* carriers in the presence of a pairing gap. Because of the pseudogap, the normal state is very different from a Fermi

liquid, where a low T upturn would otherwise be expected. Because the carrier number is effectively constant in a Fermi liquid, this upturn would derive from the decrease in inter-particle scattering. The behavior of the shear viscosity in superfluid helium-4 also shows a low T upturn. This is thought to reflect the phononic excitations which dominate the transport in this regime. In a BCS-like superfluid the collective mode phonon-like excitations are longitudinal. In a charged superconductor, as is well known, they do not affect the analogous near-zero frequency conductivity. Similarly, to the extent that the unitary Fermi gas has BCS-like characteristics, one would not expect the phonons to affect a transverse probe, like the shear viscosity. This may then explain the measured behavior of the viscosity.

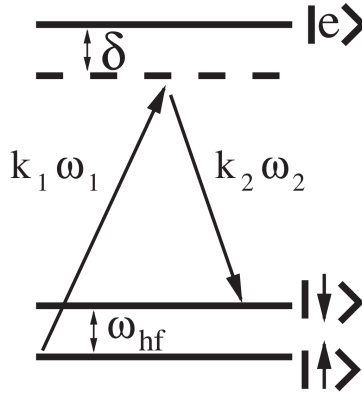*4.6. Two Photon Bragg Scattering: Analogies with Neutron Scattering Experiments*

Figure 13: Experimental Scheme for Bragg Scattering. This represents a "spin flip" process in the sense that the final state and the initial state are different. One can also contemplate non-spin flip processes in which the initial and final states correspond to the same quantum index.

The analogue to neutron experiments which have been so important in condensed matter, are two photon Bragg scattering studies. A strength of cold atom experiments is that, unlike neutron probes, they can, in principle, separately measure the density and spin correlation functions. Bragg scattering can be thought of as a coherent scattering process involving absorption of a photon from one of two laser (Bragg) beams and stimulated emission into the other: a two-photon transition. This combination of processes can

25

leave the atoms in the same internal state, but with a new momentum, k, determined by the geometry and wavelength of the Bragg beams. The two lasers have slightly different frequencies, to additionally account for a shift in energy of the final state. One can also contemplate processes where the internal states are changed such as in Figure 13. In linear response theory these experiments correspond to measuring the dynamical density-density or spin density-spin density correlation functions. These are functions of the momentum and frequency transfer. Typically, the Bragg response is measured by looking at the cloud using time-of-flight atom imaging, where the gas is suddenly released from the trap and allowed to expand before imaging.

An important aspect of the density-density scattering processes is that they reflect the phononic-like collective modes of the superfluid order parameter. This is in contrast, say, to what is referred to as "transverse" transport probes such as the shear viscosity or the conductivity. In this way, these measurements have the capability of indicating superfluid coherence [45].

4.7. Fermi Gases with Imbalanced Spin Populations

Unlike conventional superconductors, where spin-polarization is excluded by the Meissner effect, spin imbalance is a readily tunable parameter in ultracold atomic Fermi gases. Shortly after the development of the BCS theory, theorists began to speculate how pairing is modified by spin-polarization. They predicted new and exotic pairing mechanisms, such as the elusive FFLO-state (named after its proposers: Fulde, Ferrell, Larkin, and Ovchinnikov), that may occur in an imbalanced system. The FFLO-state features pairs with a momentum equal to the difference of the Fermi momenta of the two spin-states. This non-zero center-of-mass momentum results in an order parameter that is both anisotropic and oscillatory in space.

While spin-polarization is excluded in conventional superconductors, certain compounds such as the heavy-fermion materials, support coexisting superconducting and magnetic order. While there is some preliminary evidence for FFLO-pairing in these systems, the smoking gun, non-zero pair momentum, has not been found. Arbitrarily spin-polarized atomic Fermi gases may be created by simply adjusting the relative populations of the hyperfine sublevels corresponding to "spin-up" and and "spin-down". The stability of these states over the time scale (seconds) of the experiments ensures that the spin-polarization of the gas does not vary during the experiment. Several experiments have been performed in this way with the result that the gas

phase separates into an unpolarized superfluid core surrounded by a polarized normal shell [46, 47, 48]. No evidence for the FFLO state has yet been found.

The FFLO state in three dimensions (3D) remains elusive, but theory shows that it is ubiquitous in a spin-imbalanced Fermi gas in 1D [49]. The phase diagram, shown in Fig. 14, is predicted to have three distinct phases: 1) fully-polarized normal; 2) fully-paired superfluid; and 3) partially-polarized FFLO superfluid. This result was explored experimentally by using a two-dimensional optical lattice to produce an array of 1D tubes [50]. By making the lattice intensity sufficiently strong, the tubes are effectively isolated from one another. Since the atoms are confined harmonically along the tube axis, the density and hence the total chemical potential $\mu = \mu_\uparrow + \mu_\downarrow$ in each tube varies along this axis. While μ varies from a maximum value μ_0 at the center of the tube to 0 at the edges, the chemical potential difference $h = \mu_\uparrow - \mu_\downarrow$ must be constant in order for the gas to be in chemical equilibrium. Traversing the tube from center to the edge corresponds to a cut through the phase diagram, as indicated by the vertical lines in Fig. 14. If μ_0 is sufficiently large for the center of the tube to be partially polarized, a phase boundary will be encountered in passing from the center of the tube to the edge. For each combination of μ_0 and h, therefore, the tube will exhibit a pair of phases, with the center always being partially polarized while the wings will be either fully paired for small h, or fully polarized for large h.

Each tube was loaded with $\sim$200 ^{6}Li atoms with a particular imbalance. Phase boundaries were extracted from the density distributions obtained from optical imaging. The fully polarized/partially polarized boundary is determined by where the minority density $n_\downarrow$ goes to zero, while the fully paired/partially polarized boundary is given by the location of vanishing spin density $n_\uparrow - n_\downarrow$. Several representative density distributions showing the phase boundaries are given in Fig. 15. The phase diagram was mapped out experimentally in this way, and good agreement was found with Bethe-ansatz theory [50].

4.8. Rotating Gases and Analogue of Magnetic Field Effects

In contrast to a normal fluid such as water, a superfluid can only rotate by forming a regular array of quantized vortices, each of which carries part of the total angular momentum of the superfluid. In addition to expelling atoms from their centers to leave a string-like hollow core, the vortices also repel each other to form a regular lattice pattern. In trapped atomic gases,
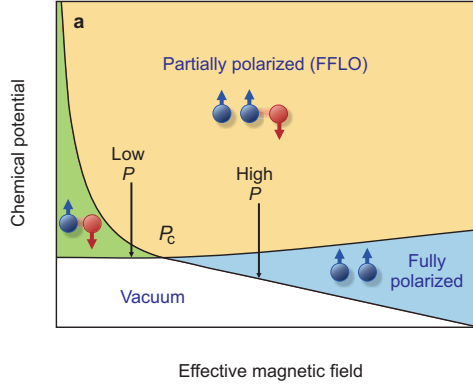
Figure 14: Phase diagram of a one-dimensional spin-imbalanced Fermi gas. The horizontal axis is the effective magnetic field h, which is related to the degree of polarization. The vertical axis is the total chemical potential μ, which is related to the density. The vertical lines show how the phase diagram is traversed in going from the center of the 1D tube, where μ) is high, to the edges of the tube. At low imbalance the edge corresponds to a fully paired phase, while for high imbalance the edge is fully polarized. In both cases, the center of the tube is partially polarized and predicted to the exotic FFLO (Fulde-Ferrell-Larkin-Ovchinnikov) paired state. (Reprinted from Ref. [50] and adapted from Ref. [49])

.

this rotation can be created by using a repulsive "spoon" potential, created by a blue-detuned laser beam, to vigorously stir the gas.

Charged fermionic superconductors and rotating superfluids are closely related by the correspondence

$$ e\boldsymbol{A}(\boldsymbol{r}) \leftrightarrow m\boldsymbol{\omega} \times \boldsymbol{r} \tag{14} $$

between the superconductor with a magnetic field and the neutral rotating (at frequency ω) superfluid. It can be said that neutral superfluids are more analogous to extreme type II superconductors, where the penetration depth is infinite. Just as in charged superconductors, at sufficiently high rotation frequencies, the neutral superfluids exhibit vortices (as in Figure 8) and these, in turn, exhibit quantized circulation.

Experiments to explore vortex phases and possible quantum Hall phenomena are underway. Some progress towards pursuing analogies with condensed matter relates to the precursor diamagnetism observed, say, in the high T_c cuprates. This diamagnetism has been the topic of considerable excitement [51] and much debate. Analogous to this diamagnetism in a charged super-
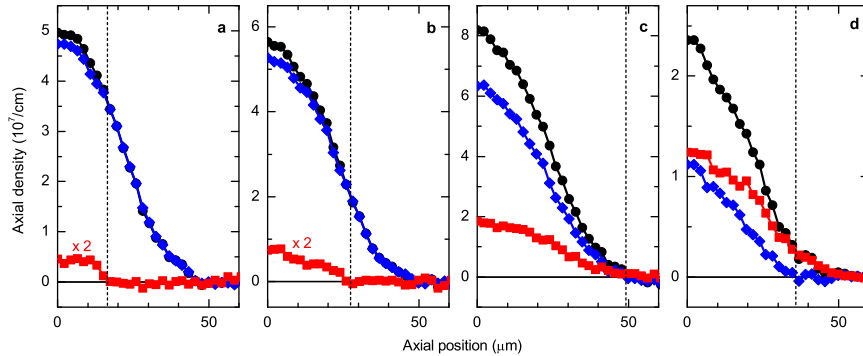
Figure 15: Axial density profiles of a spin-imbalanced 1D ensemble of tubes. Black circles represent the 1D density of the majority atoms (spin-up) , the blue diamonds represent the minority (spin-down), while the red squares show the density difference. The dashed vertical lines indicate phase boundaries, where either the minority density or the density difference vanish. The polarizations P in the central tube are (a) $P = 0.015$, (b) $P = 0.055$, (c) $P = 0.10$, and (d) $P = 0.33$. For low P (a and b), the edge of the cloud is fully paired and the difference is 0, while for larger P (d), the edge is fully polarized and the minority density vanishes. (Reprinted from Ref. [50])

.

conductor may be an above-T_c reduction in the moment of inertia of a Fermi superfluid. This is associated with finite size clouds. There may be some experimental indications that the equilibrium values of this moment of inertia are somewhat suppressed in the normal state [52]. Besides high T_c cuprates, this general class of experiments bears on other important condensed matter systems such as possible observation of supersolid phases.

5. Conclusions

The aim of this Chapter is to convey new and exciting developments in the physics of ultracold atoms to condensed matter physicists. It should be clear that, because of the shared Fermi statistics, atomic Fermi gases (and their optical lattice counterparts) have the potential for addressing important unsolved problems relating to electrons in condensed matter. They would seem even more promising in this regard than atomic Bose gases.

Another exciting aspect of the Fermi gases is their potential to explore a generalized form of fermionic superfluidity which seems, in many ways, more natural than simple BCS theory. In this generalized form, known as BCS-BEC crossover theory, the pair size must no longer be large or the pair

binding weak. As a result, pairs form at a higher temperature (called T^* in the literature) than that at which they condense, T_c. BCS theory as originally postulated can be viewed as a paradigm among theories of condensed matter systems; it is generic and model independent, and extremely well verified experimentally for conventional (presumably long coherence length) superconductors. The observation that a BCS-like approach extends beyond strict BCS theory, suggests that there is a larger theory to be discovered. Equally exciting is the possibility that this discovery phase can proceed in a very collaborative fashion, involving both theory and experiment.

One fascinating aspect feature of this crossover is that the statistics may be tuned continuously from fermionic to bosonic. This may lead to a fundamental challenge for theory. In any attempt to combine bosonic and fermionic mean field theories, as must be accomplished in BCS-BEC crossover, one should be aware that there is no fully satisfactory mean field theory of the weakly interacting Bose gas (or Bogoliubov theory) which addresses the entire range of temperatures. This is in contrast to the situation for the fermionic (BCS-based) superfluids which apply to all temperatures. The central problem is that extensions of Bogoliubov theory to the transition region generally lead to a first order transition. This suggests that either one must use a far more sophisticated model (than Bogoliubov theory) or a simpler BCS-based-level theory (in which the bosons are essentially non-interacting) to avoid discontinuities at T_c, (for example as shown in the inset to Figure 12).

The BCS-BEC crossover picture has been investigated for many years in the context of high temperature superconductors [53]. It leads to a particular interpretation of a fascinating, but not well understood non-superfluid phase, known as the "pseudogap state." In the cold atom system, this crossover description is not just a scenario, but has been realized in the laboratory. A number of cold gas experiments have been interpreted as evidence for a pseudogap state. Where there seems to be controversy about this claim is in inferences drawn from thermodynamics [36]. We note, finally, that research in this field has not been limited exclusively to the two communities (condensed matter and AMO). One has seen the application of these crossover ideas and, in particular a focus on the unitary gas, to nuclear physics and to particle physics as well. There are not many problems in physics which have as great an overlap with different subfield communities.

We have tried in this Chapter to stress the powerful tunability of the ultracold Fermi gases arising from Feshbach and other experimental "knobs." We have also emphasized the wide-ranging experimental tools which have

been developed by the AMO community over a relatively short period of time. With these tools and others awaiting development, the future is wide open.

Acknowledgements

References

[1] O'Hara, K. M., Hemmer, S. L., Gehm, M. E., Granade, S. R., and Thomas, J. E. *Science* **298**(1), 2179–2182 (2002).

[2] Anderson, M. H., Ensher, J. R., Matthews, M. R., Wieman, C. E., and Cornell, E. A. *Science* **269**, 198–201 (1995).

[3] Bradley, C. C., Sackett, C. A., Tollett, J. J., and Hulet, R. G. *Physical Review Letters* **75**, 1687 (1995).

[4] Bradley, C. C., Sackett, C. A., and Hulet, R. G. *Physical Review Letters* **78**(6), 985–989 (1997).

[5] Davis, K. B., Mewes, M.-O., Andrews, M. R., van Druten, N. J., Durfee, D. S., Kurn, D. M., and Ketterle, W. *Physical Review Letters* **75**(22), 3969 (1995).

[6] Houbiers, M. and Stoof, H. T. C. *Physical Review A* **54**, 5055 (1996).

[7] Houbiers, M., Stoof, H. T. C., McAlexander, W. I., and Hulet, R. G. *Physical Review A* **57**(3), R1497–1500 (1998).

[8] DeMarco, B. and Jin, D. S. *Science* **285**, 1703 (1999).

[9] Truscott, A. G., Strecker, K. E., McAlexander, W. I., Partridge, G. B., and Hulet, R. G. *Science* **291**, 2570–2572 (2001).

[10] Schreck, F., Khaykovich, L., Corwin, K. L., Ferrari, G., Bourdel, T., Cubizolles, J., and Salomon, C. *Physical Review Letters* **87**(8), 080403 (2001).

[11] Chin, C., Grimm, R., Julienne, P., and Tiesinga, E. *Reviews of Modern Physics* **82**, 1225–1286 (2010).

[12] E, S. K., Partridge, G. B., and Hulet, R. G. *Phys. Rev. Lett.* **91**, 080406 (2003).

[13] Greiner, M., Regal, C. A., and Jin, D. S. *Nature (London)* **426**, 537 (2003).

[14] Jochim, S., Bartenstein, M., Altmeyer, A., Hendl, G., Riedl, S., Chin, C., Denschlag, J. H., and Grimm, R. *Science* **302**, 2101 (2003).

[15] Regal, C. A., Greiner, M., and Jin, D. S. *Phys. Rev. Lett.* **92**(1), 040403–040406 (2004).

[16] Zwierlein, M. W., Stan, C. A., Schunck, C. H., Raupach, S. M. F., Kerman, A. J., and Ketterle, W. *Phys. Rev. Lett.* **92**, 120403 (2004).

[17] Kinast, J., Turlapov, A., Thomas, J. E., Chen, Q. J., Stajic, J., and Levin, K. *Science* **307**, 1296–1299 (2005). Published online 27 January 2005; doi:10.1126/science.1109220.

[18] Zwierlein, M. W., Abo-Shaeer, J. R., Schirotzek, A., and Ketterle, W. *Nature (London)* **435**, 170404 (2005).

[19] Eagles, D. M. *Phys. Rev.* **186**(2), 456–63 (1969).

[20] Leggett, A. J. In *Modern Trends in the Theory of Condensed Matter*, Pekalski, A. and Przystawa, J., editors, 13–27 (Springer-Verlag, Berlin, 1980).

[21] Törmä, P. and Zoller, P. *Phys. Rev. Lett.* **85**, 487 (2000).

[22] Bruun, G. M., Torma, P., Rodriguez, M., and Zoller, P. *Phys. Rev. A* **64**, 033609 (2001).

[23] Chin, C., Bartenstein, M., Altmeyer, A., Riedl, S., Jochim, S., Hecker-Denschlag, J., and Grimm, R. *Science* **305**, 1128–1130 (2004).

[24] Kinnunen, J., Rodriguez, M., and Törmä, P. *Science* **305**, 1131–1133 (2004).

[25] Stajic, J., Milstein, J. N., Chen, Q. J., Chiofalo, M. L., Holland, M. J., and Levin, K. *Phys. Rev. A* **69**, 063610 (2004).

[26] Shin, Y. I., Schunck, C. H., Schirotzek, A., and Ketterle, W. *Phys. Rev. Lett* **99**, 090403 (2007).

[27] Stewart, J. T., Gaebler, J. P., and Jin, D. S. *Nature* **454**, 744 (2008).

[28] Gaebler, J. P., Stewart, J. T., Jin, D. S., Perali, A., Pieri, P., and Strinati, G. C. *Nature Physics* **6**, 569 (2010).

[29] Tan, S. *Annals of Physics* **323**, 2952–2970 (2008).

[30] Tan, S. *Annals of Physics* **323**, 2971–2986 (2008).

[31] Braaten, E., Kang, D., and Platter, L. *Physical Review A* **78**, 053606–1–19 (2008).

[32] Partridge, G. B., Strecker, K. E., Kamar, R. I., Jack, M. W., and Hulet, R. G. *Physical Review Letters* **95**(2), 020404–1–4 (2005).

[33] Werner, F., Tarruell, L., and Castin, Y. *European Physical Journal B* **68**, 401 (2009).

[34] Zhang, S. and Leggett, A. J. *Phys. Rev. A* **79**, 023601 (2009).

[35] Stewart, J. T., Gaebler, J. P., Drake, T. E., and Jin, D. S. *Physical Review Letters* **104**, 235301 (2010).

[36] Nascimbene, S., Navon, N., J, J. K., Chevy, F., and Salomon, C. *Nature* **463**, 1057 (2010).

[37] Horikoshi, M., Nakajima, S., Ueda, M., and Mukaiyama, T. *Science* **327**, 442 (2010).

[38] Ku, M. J. H., Sommer, A., Cheuk, L., and Zwierlein, M. e-print ArXiv:1110.3309, (2006).

[39] Hu, H., Drummond, P. D., and Liu, X. J. *Nature Phys.* **3**, 469 (2007).

[40] Nozières, P. and Schmitt-Rink, S. *J. Low Temp. Phys.* **59**, 195–211 (1985).

[41] Guo, H., Wulin, D., Chien, C.-C., and Levin, K. *New Journal of Physics* **13**, 0i75011–075043 (2011).

[42] Emery, V. J. and Kivelson, S. A. *Nature (London)* **374**(6521), 434–7 (1995).

[43] Cao, C., Elliott, E., Joseph, J., Wu, H., Petricka, J., Schafer, T., and Thomas, J. E. *Science* **331**, 58 (2011).

[44] Guo, H., Wulin, D., Chien, C.-C., and Levin, K. *Phys. Rev. Lett.* **107**, 020403 (2011).

[45] Guo, H., Chien, C.-C., and Levin, K. *Phys. Rev. Lett.* **105**, 120401 (2010).

[46] Zwierlein, M. W., Schirotzek, A., Schunck, C. H., and Ketterle, W. *Science* **311**, 492–6 (2006).

[47] Partridge, G. B., Li, W., Kamar, R. I., Liao, Y.-a., and Hulet, R. G. *Science* **311**, 503–5 (2006).

[48] Nascimbène, S., Navon, N., Jiang, K. J., Tarruell, L., Teichmann, M., McKeever, J., Chevy, F., and Salomon, C. *Physical Review Letters* **103**, 170402 (2000).

[49] Orso, G. *Physical Review Letters* **98**, 070402 (2007).

[50] Liao, Y.-A., Rittner, A. S. C., Paprotta, T., Li, W., Partridge, G. B., Hulet, R. G., Baur, S. K., and Mueller, E. J. *Nature* **467**, 567–569 (2010).

[51] Wang, Y., Xu, Z. A., Kakeshita, T., Uchida, S., and Ong, N. P. *Phys. Rev. B* **64**(22), 224519 (2001).

[52] Riedl, S., Sanchez Guajardo, E. R., Kohstall, C., Denschlag, J. H., and Grimm, R. *New Journal of Physics* **13**, 035003 (2011).

[53] Chen, Q. J., Stajic, J., Tan, S. N., and Levin, K. *Phys. Rep.* **412**(1), 1–88 June (2005).